Comparison of *in vivo* vs. *ex situ* obtained material properties of sheep common carotid artery

Marija Smoljkić[a,*], Peter Verbrugghe[b], Matilda Larsson[c,d], Erik Widman[c,d], Heleen Fehervary[a], Jan D'hooge[e], Jos Vander Sloten[a], Nele Famaey[b,*]

[a] *Biomechanics Section, Mechanical Engineering Department, KU Leuven, Leuven, Belgium*
[b] *Clinical Cardiac Surgery, Department of Cardiovascular Sciences, KU Leuven, Leuven, Belgium*
[c] *School of Technology and Health, Department of Medical Engineering, KTH Royal Institute of Technology, Stockholm, Sweden*
[d] *Department of Molecular Medicine and Surgery, Karolinska Institutet, Stockholm, Sweden*
[e] *Cardiovascular Imaging and Dynamics, Department of Cardiovascular Sciences, KU Leuven, Leuven, Belgium*

Abstract

Patient-specific biomechanical modelling can improve preoperative surgical planning. This requires patient-specific geometry as well as patient-specific material properties as input. The latter are, however, still quite challenging to estimate *in vivo*.

This study focuses on the estimation of the mechanical properties of the arterial wall. Firstly, *in vivo* pressure, diameter and thickness of the arterial wall were acquired for sheep common carotid arteries. Next, the animals were sacrificed and the tissue was stored for mechanical testing. Planar biaxial tests were performed to obtain experimental stress-stretch curves. Finally, parameters for the hyperelastic Mooney-Rivlin and Gasser-Ogden-Holzapfel (GOH) material model were estimated based on the *in vivo* obtained pressure-diameter data as well as on the *ex situ* experimental stress-stretch curves.

Both material models were able to capture the *in vivo* behaviour of the tissue. However, in the *ex situ* case only the GOH model provided satisfactory results. When comparing different fitting approaches, *in vivo* vs. *ex situ*, each of them showed its own advantages and disadvantages. The *in vivo* approach

*Corresponding author
Email addresses: nele.famaey@kuleuven.be (Nele Famaey)

estimates the properties of the tissue in its physiological state while the *ex situ* approach allows to apply different loadings to properly capture the anisotropy of the tissue. Both of them could be further enhanced by improving the estimation of the stress-free state, i.e. by adding residual circumferential stresses *in vivo* and by accounting for the flattening effect of the tested samples *ex vivo*.

- Competing interests: none declared

- Word count: 4716

Key words: common carotid artery, material properties, constitutive modelling, parameter estimation

---

1. Introduction

Preoperative planning can be of critical importance and often determine the outcome of a surgical procedure. Without doubt, this process should be as patient-specific as possible. Patient-specific anatomical geometry is already used in the clinic for orthopaedic procedures (e.g. hip [1, 2] and knee arthroplasty [3, 4]), dental implants [5, 6], reconstructive surgery [7, 8], etc. In cardiovascular surgery, the most prominent applications are stenting procedures [9, 10, 11], valve replacements [12] and aneurysm repair [13].

In the case of soft tissue procedures, the intra-operative 'work space' will deform with respect to the preoperative plan. The numerical simulations that are employed to estimate these deformations require, besides geometrical information, information on the mechanical behaviour of the tissue. Despite the large inter-patient variability, to date, the mechanical properties used in these simulations are not yet patient-specific. The reason for this is that, for most biological tissues, estimating the material properties is still a very challenging task, far less straightforward than obtaining the patient-specific geometry. This is mainly due to the destructive nature of classical mechanical testing, whereas

the estimation should be performed *in vivo* in a non- or at least minimally invasive manner, to allow incorporation into a clinical work flow. These constraints limit the possible measurement techniques, while the tissue to be characterized is complex, nonlinear and anisotropic.

The constitutive behavior of cardiovascular tissue is generally described using hyperelastic material models. Most commonly, parameters are obtained through *ex situ* uniaxial [14], planar biaxial [15] or inflation-extension testing [16]. A number of studies have reported *in vivo* estimated parameters of nonlinear anisotropic material descriptions for arterial tissue [17, 18, 19]. However, these methods and the reported parameters have not been validated. In previous work from our group [20], as well as in the study done by Wittk et al. [21], methods were proposed for non-invasive assessment and were subsequently verified *in silico* using simulated datasets. Nevertheless, to the authors' knowledge, a validation in the form of an experimental comparison between material parameters obtained *in vivo* and those obtained *ex situ* with standard material characterization approaches has never been performed.

The *ex situ* experimental parameter estimation is the gold standard for estimation of constitutive parameters. In this study, the goal was to compare the parameters obtained with *in vivo* and *ex situ* techniques. Invasive and non-invasive material property estimation was performed on the common carotid artery (CCA) of three sheep. First, all necessary data such as diameter, pressure and arterial wall thickness were acquired *in vivo*. After euthanasia, the CCAs were excised and stored for *ex situ* planar biaxial mechanical testing. Constitutive material properties were estimated both from the *in vivo* obtained pressure-diameter curves and the *ex situ* experimental stress-stretch curves. The following section describes the *in vivo* and *ex situ* data acquisition process as well as subsequent parameter estimation. In the last two sections, the results are presented and the performance of both approaches are discussed and compared.

2. Materials and Methods

2.1. In vivo measurements

2.1.1. Animal preparation

The experiments were performed in accordance with the Guide for the Care and Use of Laboratory Animals published by the U.S. National Institutes of Health (NIH Publication No. 85-23, revised 1996). Ethical approval was obtained from the local ethics committee (Animal Ethics Committee of KU Leuven, Leuven, Belgium). In this study, three one-year-old female Swifter sheep were used. Injections of Ketamine (15 mg kg^{-1}) and xylazine (2%, 0.01 ml kg^{-1}) were used to sedate the animals. Anaesthesia was maintained with isoflurane (2-4%). Throughout the procedure, heart rate, blood pressure, end-tidal CO_2, and blood O_2- saturation were monitored. Drugs were administered via an intravenous line which was inserted in an extremity vein and via an arterial line in the ear. The animals were positioned on the surgical table in a supine position and all measurements were performed on the left and right common carotid artery (CCA). Table 1 provides an overview of the animals and their physiological parameters.

Table 1: Characteristics of the three one-year-old female Suffolk sheep included in the study. BP stands for blood pressure.

Sheep	Weight [kg]	Heart rate [bpm]	Diastolic BP [mmHg]	Systolic BP [mmHg]
S1	54	66	89.2	112.5
S2	51	66	45.7	67.5
S3	44	70	46.1	65.3

2.1.2. Data acquisition

All *in vivo* data was collected either minimally invasively or non-invasively. Minimally invasive pressure measurements were performed with a Mikro-cath®

cardiology catheter equipped with a Mikro-tip® pressure transducer (Millar Instruments, Houston, USA).

Diameter and intima-media wall thickness (IMT) were measured using a Vivid7® ultrasound system (GE Healthcare, Horten, Norway) with a linear-array transducer (12L) at a center frequency of 12 MHz and a sampling frequency of 40 MHz. Both long-axis and short-axis images of the left and right CCA were acquired. Through three cardiac cycles, images were acquired using free-hand scanning at a frame rate of 45.3 frames s^{-1} with a line density of 13.9 lines mm^{-1} in the grayscale image. The image width was 27 mm, whereas the image depth was 30 mm. The focus point was positioned in the posterior wall of the artery.

Ultrasound imaging was done on both left and right side, followed by the minimally invasive pressure measurements. The Millar® pressure catheter was introduced in the left CCA to obtain pressure. Finally, the ultrasound imaging was repeated to check for the effect of catheter insertion. Speckle tracking motion estimation was performed on the radio frequency data using a previously developed algorithm based on normalized cross-correlation [22, 23]. Axial motion estimation (along the ultrasound beam) was performed on the walls of the CCA to measure the change in diameter throughout the cardiac cycle. For a detailed description of the algorithm the reader is referred elsewhere ([22, 23]). On sheep S3, all measurements were performed only on the left CCA.

The *in vivo* pressures and diameters were not simultaneously acquired so the manual synchronization was done as a part of post-processing using Matlab® R2015a (The Math-Works, Natick, MA, USA). The signals were synchronized by matching the maximal diameter to the maximal pressure and minimizing the hysteresis in the pressure-diameter loop. Figure 1 shows an example of synchronized loading pressure-diameter curves. The original curve contains an irregular, non-convex part which is typical for CCAs. However the material models used in this study are not able to model this behaviour. For that reason, that part of the curve was left out and only the blue dotted line on Figure 1 was further used. The origin of this non-convex part comes from the fact the

pressure wave at any given location is a result of two waves. The incident wave (in the direction of the blood flow) and the reflected wave (in the direction opposite to the blood flow). The reflected wave comes, among other things, from bifurcations [24]. The CCA is close to a bifurcation which influences the waveform and produces the mentioned non-convex part.

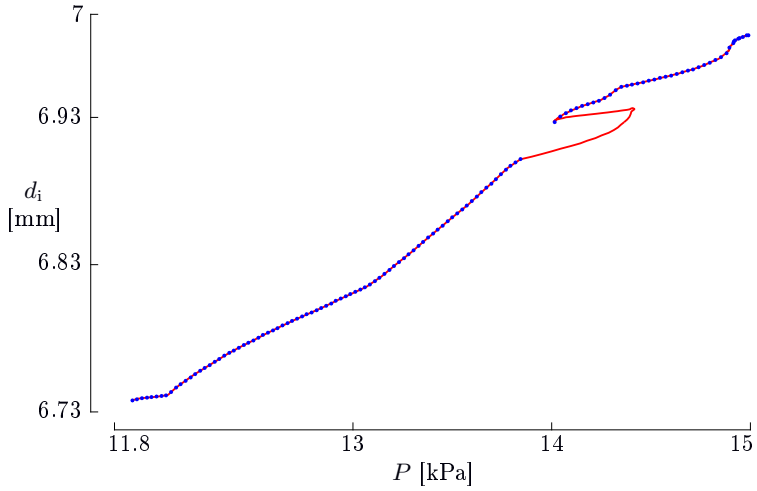

Figure 1: Pressure-inner diameter curve for S1 right CCA. The full line shows the original curve after the manual synchronization. The dotted line shows the curve used as an input for parameter estimation.

2.2. Ex situ experiments

2.2.1. Sample preparation

After completing the *in vivo* measurements, the animals were sacrificed using high-dose pentobarbital and potassium. The left and right CCA were exposed and a surgical suture wire was placed at two ends to mark the *in situ* segment length. After excision, the *ex vivo* length was measured. The ratio of these two values provided an estimate of the *in vivo* axial prestretch. The arterial segments were then submerged in a phosphate buffered saline (PBS) solution and cryopreserved at -80°C.

Prior to planar biaxial testing, the samples were slowly thawed overnight at +4°C. Each sample was fully tested over a time span of one day. The samples

were cut in squares of 8x8 mm. The thickness of each sample was measured optically, by imaging it while placed between two metal plates of known thickness (see Figure 2a). Small fragments of surgical suture wire were used as markers, five of which were glued in the central region (Figure 2b) where the stresses are reported to be the most homogeneous [25].

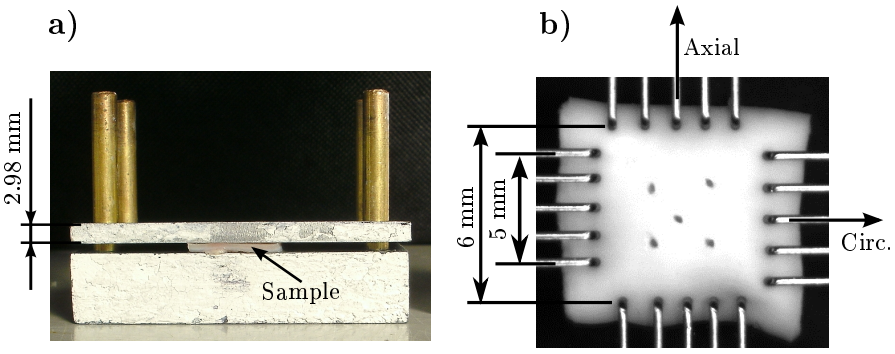

Figure 2: a) *Ex situ* thickness measurement of a sample (prior to marker placement and testing); b) a sample mounted for planar biaxial testing. Circ. stands for circumferential direction.

2.2.2. Data acquisition

All samples were tested on a planar biaxial testing device specifically designed for the mechanical testing of biological soft tissue (BioTester® 5000, CellScale, Waterloo, Canada). The system is equipped with two 23 N load cells with an accuracy of 50 mN. Samples were mounted using rakes and the size covered by rakes was 6x6 mm. The circumferential and axial directions were aligned with the testing axes of the setup. During the experiments, the samples were submerged in a 0.9% NaCl fluid bath. The fluid bath was heated to 37°C. The built-in CCD camera (resolution 1280x960 pixels) monitored the deformation of the tissue, and therefore the displacements of the markers, during the test. Forces and images and were stored at a frequency of 30 Hz. An in-house developed Matlab® script was used for tracking the markers in the images.

A force-controlled testing protocol was applied. The applied force (F_θ^{sys}) was estimated from the physiological loading state. For a healthy sheep a value

of 100 mmHg (0.013 MPa) is assumed for the systolic pressure, from which the physiological circumferential stress can be roughly estimated via Laplace's law as $\sigma_\theta = P\ d_\mathrm{i}/2\ h$ with physiological pressures P, the corresponding inner diameters d_i and the wall thickness h. The circumferential force F_θ was calculated as $F_\theta = \sigma_\theta\ w\ t$, where w and t are the planar biaxial sample width and thickness respectively. According to recommendations for stress calculations reported by Fehervary et al. [26], the length covered by the rakes was used as a sample width. For the values reported in Table 2 and with an assumption that $t = h$, a physiological F_θ^{sys} was estimated to be 0.26 N and F_θ^{dias} to be 0.18 N. Assuming an average heart rate of 75 bpm for healthy sheep, the loading rate was calculated as the difference in force multiplied by the average heart rate in seconds $(F_\theta^{sys} - F_\theta^{dias}) * 75/60$ [N/s].

Table 2: Values of the physiological pressure P, inner diameter d_i and planar biaxial sample size w (see Figure 2b) used for calculation of the *in vivo* circumferential force F_θ at diastolic and systolic level. The values are comparable to the dimensions of sheep CCAs measured in this study.

	P [mmHg]	d_i [mm]	w [mm]	F_θ [N]
Diastolic	80	5.76	6	0.18
Systolic	100	6.48	6	0.26

The testing protocol started with ten preconditioning cycles up to 0.09 N (half of the F_θ^{dias}) with a loading rate of 0.1 N/s. Every cycle started with a preload of 70 mN to exceed the noise level of the load cells. Each specimen was subjected to three different circumferential to axial force ratios: 1:1, 1:0.5 and 0.5:1. For each ratio, five testing cycles were applied. Four different force levels were used, namely 1x, 3x, 6x and 9x F_θ^{sys}. The highest reached force level before failure of a sample was used for parameter estimation, i.e. 6xF_θ^{sys}. Loading curves from the fifth cycle of all three ratios were used.

2.3. Material models

Two hyperelastic constitutive material models were used in this study, the isotropic Mooney-Rivlin model and the anisotropic Gasser-Ogden-Holzapfel model. In both cases, the tissue is considered to be incompressible. From that assumption it follows that radial, circumferential and axial principal stretches are related through $\lambda_r \lambda_\theta \lambda_z = 1$.

2.3.1. Mooney-Rivlin model

The used two-parameter Mooney-Rivlin (MR) strain energy density function (SEDF) is expressed as follows:

$$\begin{aligned} \Psi &= c_1(I_1 - 3) + c_2(I_2 - 3), \\ I_1 = \lambda_r^2 + \lambda_\theta^2 + \lambda_z^2, &\qquad I_2 = \lambda_r^2\lambda_\theta^2 + \lambda_\theta^2\lambda_z^2 + \lambda_z^2\lambda_r^2, \end{aligned} \tag{1}$$

where, c_1 and c_2 are stress-like material constants. I_1 and I_2 are the first and the second strain invariant of the right Cauchy-Green strain tensor.

2.3.2. Gasser-Ogden-Holzapfel model

The second used constitutive model was proposed by Gasser et al. [27] and is further referred to as the GOH model. This model is a combination of an isotropic and an anisotropic part, which model the strain energy stored in the matrix material and in the collagen fibres, respectively as

$$\Psi = \Psi_{mat} + \Psi_{col}. \tag{2}$$

The isotropic matrix contribution is represented by a Neo-Hookean model

$$\Psi_{mat} = \frac{\mu}{2}(I_1 - 3), \qquad I_1 = \lambda_r^2 + \lambda_\theta^2 + \lambda_z^2. \tag{3}$$

The stress-like parameter μ represents the stiffness of the matrix material and I_1 is the first invariant of the right Cauchy-Green strain tensor (Eq. 3b).

The anisotropic collagen fibre contribution is expressed with the exponential function. If the presence of two symmetrically oriented collagen fibre families is assumed, and the shear stresses are considered to be negligible, the collagen contribution can be expressed as

$$\Psi_{col} = \frac{k_1}{2k_2} \sum_{i=4,6} \Big\{ \exp\big\{ k_2[(\kappa I_1 + (1-3\kappa)I_i) - 1]^2 \big\} - 1 \Big\}, \qquad I_{4,6} = \lambda_z^2 \sin^2\alpha + \lambda_\theta^2 \cos^2\alpha. \tag{4}$$

I_4 and I_6 are the fourth and the sixth strain invariant, respectively, each corresponding to one fibre family. Due to the symmetry and no shear assumptions, they are identical (Eq. 4b). Parameters k_1 and k_2 reflect the mechanical properties of the collagen fibre families. k_1 is a stress-like parameter describing the fibre stiffness and k_2 is a dimensionless parameter related to the stiffening of the collagen fibres at higher pressures. Parameter α defines the fibre angle defined w.r.t. the circumferential direction. κ incorporates the dispersion of the fibres around the main orientation described with α. κ is a positive number between 0 (no dispersion) and 1/3 (isotropic dispersion). For cases where k_2 goes to very low values, Eq. 2 can be further simplified and in that case does not contain parameter k_2, $\Psi_{col} = \frac{k_1}{2} \sum_{i=4,6} \big(I_i - 1\big)^2$ [28].

2.4. Material parameter identification methods

The general approach to obtain the material model parameters is to minimize the difference between the measured values and the same values predicted by the constitutive model. This iterative process was performed in Matlab® R2015a, with the *lsqnonlin* routine and the *trust-region-reflective* optimization algorithm. Scaling of the parameters ensured the same search area for each parameter. Twenty initial parameter sets were given as initial points (*Multistart* function), distributed over the entire fitting range.

2.4.1. In vivo

In the *in vivo* case, the fitting approach proposed by Smoljkic et al. [20] was used briefly summarized next. Ideally, the fitting algorithm would minimize

the differences between the measured and modelled load predictions along two directions. However, only pressure can be measured *in vivo*. To compensate for the lack of axial load measurements, three additional physiologically-based conditions are introduced in the minimized objective function. The first condition is that the reduced axial force acting on the tissue is constant in the physiological pressure range. Aside from the force condition, two more energy-based conditions were implemented. The first one is related to the energy across the arterial wall which is assumed to be approximately constant. The second condition states that at diastolic pressure, the amount of energy stored in the collagen fibres is close to the amount of energy stored in the matrix material. These three conditions result in the following objective function:

$$\min \sum_{j=1}^{n} \left\{ \left[w_p \Big(P_j^{mod} - P_j^{exp} \Big) \right]^2 + \left[w_f \Big(\frac{F_j^{mod}}{A_j^{mod}} - \frac{F^{average}}{A_j^{mod}} \Big) \right]^2 \right\} + \sum_{k=1}^{m} \left\{ \left[w_{\Psi_1} \Big(\Psi_k^{dias,mod} - \Psi^{average} \Big) \right]^2 + \left[w_{\Psi_2} \Big(\Psi_{k,col}^{dias,mod} - \Psi_{k,mat}^{dias,mod} \Big) \right]^2 \right\}. \tag{5}$$

For the MR model, it is not possible to distinguish between the collagen and matrix contribution so the last condition is omitted. In the MR case, the fitted parameters were the two model parameters plus two geometrical parameters: thickness of the arterial wall in the unloaded configuration (H) and the axial prestretch (λ_z). In the GOH case, the vector contains five GOH-model parameters plus two geometrical parameters H and λ_z. P_j^{exp} is the pressure measured *in vivo* with the Millar pressure catheter. P_j^{mod} and F_j^{mod} are the pressures and forces predicted by the constitutive model for every j-th data record, as follows:

$$P_j^{mod} = \int_{\lambda_o}^{\lambda_i} (\lambda_\theta^2 \lambda_z - 1)^{-1} \frac{\partial \Psi}{\partial \lambda_\theta} d\lambda_\theta, \tag{6}$$

$$F_j^{mod} = \pi \rho_i^2 (\lambda_{\theta,i}^2 \lambda_z - 1) \int_{\lambda_o}^{\lambda_i} (\lambda_\theta^2 \lambda_z - 1)^{-2} \left(2\lambda_z \frac{\partial \Psi}{\partial \lambda_z} - \lambda \frac{\partial \Psi}{\partial \lambda_\theta} \right) \lambda_\theta d\lambda_\theta. \tag{7}$$

λ_i and λ_o are the circumferential stretches at the inner and the outer wall, respectively. The circumferential stretches are calculated as $\lambda_\theta = r/\rho$. ρ_i is the inner radius in the unloaded configuration. A_j^{mod} is the current cross-sectional area calculated as:

$$A_j^{mod} = \pi[(R_o\lambda_{o,j})^2 - (R_i\lambda_{i,j})^2]. \tag{8}$$

In (5), $F^{average}$ is calculated by using a *polyfit* function in Matlab and fitting a zero order polynomial to $\boldsymbol{F}^{mod}$. $\Psi_k^{dias,mod}$ is the strain energy density at diastole across the wall thickness. k represents different points throughout the wall going from 1 to m, m being 11 in this case. $\Psi^{average}$ is calculated by using the *polyfit* function again, but now on $\Psi^{dias,mod}$. $\Psi_{k,col}^{dias,mod}$ is the energy stored in collagen and $\Psi_{k,mat}^{dias,mod}$ is the energy contribution from the matrix material. The weighting factors depend on the chosen units and were set to ensure reasonable priorities to the constraints. Pressure, as the only measurable variable, has the highest priority. The values of the weighting factors were chosen to be 1 for w_p, 10^{-2} for w_f, 10^{-4} for w_{Ψ_1} and 10^{-1} for w_{Ψ_2}.

$\sin\alpha$ was fitted instead of α to have a more equally distributed search area for the parameters. The upper and lower boundary for α were changed accordingly. Circumferential residual stresses were not taken into account directly, but indirectly through the constraint on the strain energy through the wall thickness. For more details about the *in vivo* fitting approach, the interested reader is referred to the study by Smoljkic et al. [20].

2.4.2. Ex situ

In the *ex situ* case, the material parameters can be determined through a non-linear least square optimization procedure by comparing the circumferential ($\boldsymbol{\sigma}_{\theta\theta}^{mod}$) and axial ($\boldsymbol{\sigma}_{zz}^{mod}$) model stresses to the experimentally obtained stresses ($\boldsymbol{\sigma}_{\theta\theta}^{exp}$ and $\boldsymbol{\sigma}_{zz}^{exp}$):

$$\min \sum_{j=1}^{n} \left[(\sigma_{\theta\theta,j}^{mod} - \sigma_{\theta\theta,j}^{exp})^2 + (\sigma_{zz,j}^{mod} - \sigma_{zz,j}^{exp})^2 \right]. \tag{9}$$

In the above equation, j stands for the number of recorded data points. Experimental Cauchy stresses $\boldsymbol{\sigma}^{exp}$ are calculated from the first Piola-Kirchhoff stress $\boldsymbol{\mathcal{P}}^{exp}$g and the deformation gradient $\boldsymbol{\mathcal{F}}$ as

$$\boldsymbol{\sigma}_{qq}^{exp} = \boldsymbol{\mathcal{P}}_{qq}^{exp}\boldsymbol{\mathcal{F}}^{\mathrm{T}}, \quad \boldsymbol{\mathcal{P}}_{qq}^{exp} = \frac{\mathbf{F}_q}{\mathrm{A}_{q,0}}, \quad q = \theta, z. \tag{10}$$

$\boldsymbol{\mathcal{F}}$ is equal to $\mathrm{diag}(\lambda_r, \lambda_\theta, \lambda_z)$. $\boldsymbol{\mathcal{P}}^{exp}$ is obtained by dividing the experimentally measured forces $\mathbf{F}_q$ by the initial cross-sectional surface $\mathrm{A}_{q,0}$ (Eq. 10b). In both circumferential and axial direction, $\mathrm{A}_{q,0} = w\,t$, where w is the width covered by the rakes (6 mm as marked on Figure 2a) and t is the initial sample thickness (reported in Table 3) measured by the thickness measuring device (see Figure 2a).

Cauchy stresses predicted by the constitutive models are calculated from either Eq. 1 or Eq. 2 as

$$\boldsymbol{\sigma}_{qq,j}^{\mathrm{mod}} = \lambda_q \frac{\partial \Psi}{\partial \lambda_q} - p, \quad q = \theta, z. \tag{11}$$

The hydrostatic pressure p can be calculated from the assumption that $\boldsymbol{\sigma}_{rr} = 0$, (see Ogden [29]). More details about the material parameter estimation from a planar biaxial test can be found elsewhere [26].

The parameters were estimated with three different approaches. In the first one, data from the full tested range was used from all tested ratios (full range). Secondly, only measurements up to the systolic stress estimated with Laplace's law were used, again from all three tested ratios (physiological range). Finally, only data in the physiological range and for 1:0.5 ratio, which is assumed to be present *in vivo*, was used for the parameter estimation (physiological range & ratio).

3. Results

3.1. Thickness and axial prestretch

Table 3 reports *in vivo* as well as *ex vivo* measurements of the aortic wall thickness. The table also includes the *in situ* measurements of the axial pre-

stretch λ_z. The abbreviations in Table 3 and further on in the text stand for the different animals (S1, S2 or S3) and L and R for the measurements performed on left or right CCA. Measurements on S1L CCA were discarded from the study due to insufficient quality of the data.

Table 3: *In vivo* measurements of the intima-media thickness (IMT) at diastole (dias) and systole (sys) measured from echography images, *ex vivo* measurements of the intima-media-adventitia thickness (IMAT) measured with the thickness device showed on Figure 2a and *in situ* axial prestretch λ_z. Note that IMAT and H (obtained through fitting) might be easily confused with each other since they both refer to an unloaded thickness. However, H is the unloaded thickness in the cylindrical shape, so the residual stresses are not released yet. IMAT is the unloaded thickness of a radially cut and flattened sample. Also, H refers to the intima-media thickness, while IMAT also takes the thickness of the adventitia into account.

	In vivo		*Ex vivo*	
	$\mathrm{IMT_{dias}}$ [mm]	$\mathrm{IMT_{sys}}$ [mm]	IMAT [mm]	λ_z [-]
S1R	0.39	0.31	1.16	1.29
S2L	0.39	0.31	0.96	1.27
S2R	0.36	0.28	0.96	1.22
S3L	0.41	0.33	1.55	1.43

3.2. Material parameters

3.2.1. Mooney-Rivlin

In the case of the *in vivo* parameter estimation, four parameters were fitted for the MR model (c_1, c_2, H, λ_z). In the *ex situ* case, only two parameters were fitted, namely c_1 and c_2. Table 4 contains results for both fitting approaches.

Figure 3 shows the experimental diameter-pressure curve and the MR model prediction of it as well as the predicted reduced axial force for S1R. In the *in situ* case, based on the low R^2 values reported in Table 4, it is obvious that the model was not able to capture the complex behaviour of the carotid aortic wall for any of the three fitting approaches (full range, physiological range and physiological

Table 4: Results of the *in vivo* and *ex situ* parameter estimation for the Mooney-Rivlin model. In the *in vivo* case, for each animal, two sets of parameters are given. In the first set, all four parameters were fitted. To obtain the second set, λ_z was fixed to the measured value and the other three parameters were fitted. In the *ex situ* case, parameters were estimated in three ways. The physiological range is estimated based on the systolic pressure and 1:0.5 ratio is considered to be a physiological ratio. The coefficient of determination R^2 indicates the goodness of fit.

		c_1 [kPa]	c_2 [kPa]	H [mm]	λ_z [-]	R^2
S1R						
in vivo	λ_z fitted	115.3	37.4	0.57	1.76	0.99
	λ_z fixed	84.6	50.9	0.49	1.29	0.99
ex situ	full range	0	19.8	-	-	0.23
	physiological range	0	14.7	-	-	0.73
	physiological range and ratio	20.7	0	-	-	0.3
S2L						
in vivo	λ_z fitted	51.1	26.3	0.54	1.40	0.97
	λ_z fixed	46.6	28.9	0.51	1.27	0.96
ex situ	full range	4.8	23.8	-	-	0.44
	physiological range	0	16.7	-	-	0.59
	physiological range and ratio	28.8	0	-	-	0.67
S2R						
in vivo	λ_z fitted	34.6	22.0	0.49	1.26	0.99
	λ_z fixed	33.7	22.6	0.49	1.22	0.99
ex situ	full range	0	25.5	-	-	0.33
	physiological range	0	16.7	-	-	0.51
	physiological range and ratio	31.7	0	-	-	0.67
S3L						
in vivo	λ_z fitted	45.5	21.2	0.57	1.47	0.99
	λ_z fixed	44.4	21.8	0.57	1.43	0.99
ex situ	full range	4.3	12.2	-	-	0.23
	physiological range	3.6	7.3	-	-	0.83
	physiological range and ratio	5.4	6.7	-	-	0.77

range & ratio). This is visualized for S3 on Figure 4 where the experimental stress-strain curves are shown together with their model predictions.

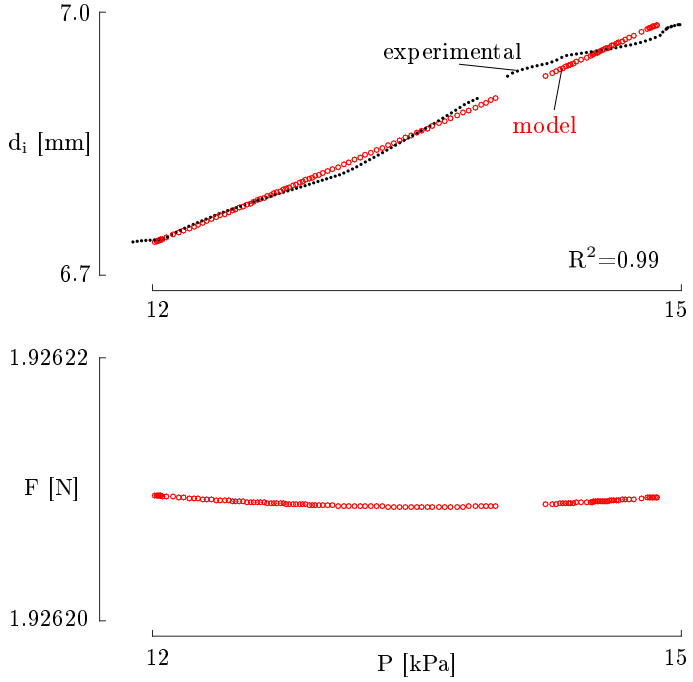

Figure 3: Results of the Mooney-Rivlin non-invasive fit for S1R. At the top, the *in vivo* measured pressure (P) and the inner diameter (d_i) data (dotted line) and the model fit (circles). Below, reduced axial force (F) predicted by the MR model.

3.2.2. Gasser-Ogden-Holzapfel

285 In the case of the *in vivo* GOH parameter estimation, seven parameters were fitted (c, k_1, k_2, α, κ, H, λ_z). In the *ex situ* case, only the first five parameters needed to be estimated, i.e. the GOH material parameters.

The *in vivo* and *ex situ* parameters of the GOH material model are shown in Table 5. The model was able to capture the nonlinear behaviour of the arterial 290 tissue in both cases. Figure 5a shows an example of an *in vivo* pressure-diameter curve together with the model prediction of it. The experimental stretch-stress curves and their model predictions are shown for S1R CCA on Figure 6.

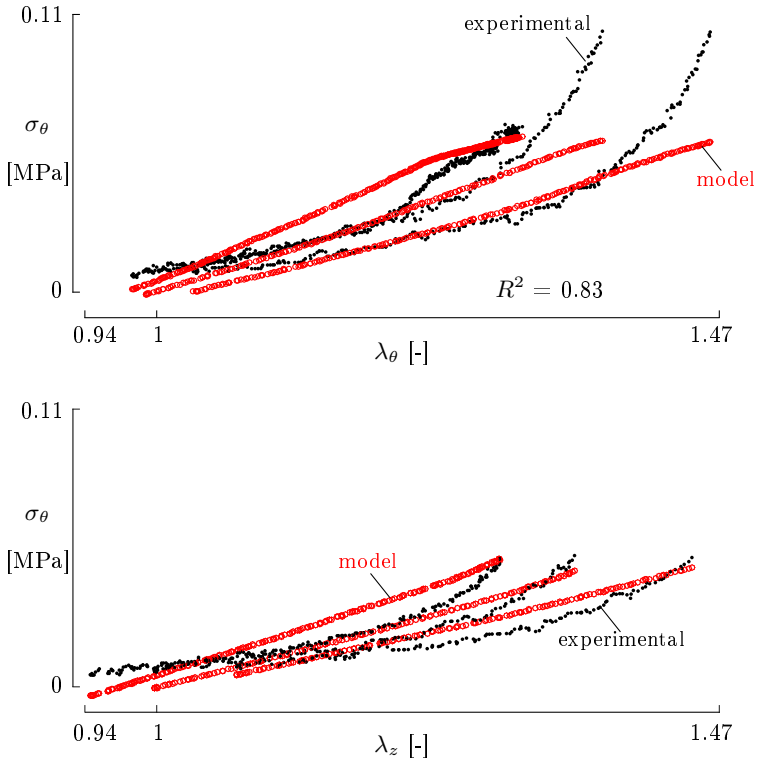

Figure 4: Experimental stress-stretch curves from zero to the physiological systolic stress level (dotted lines) and MR model fit (circles) from S3L CCA. All three tested ratios are plotted.

4. Discussion

In this study, diameter, pressure and wall thickness were measured *in vivo* on three sheep CCA. This data was used for material parameter estimation of two hyperelastic constitutive models, MR and GOH. After excision, the tissue was mechanically tested using a planar biaxial setup, based on which the same material parameters were estimated from the experimental stress-stretch curves. To the authors' knowledge this study, together with that of Smoljkic et al. [30], one of the first two studies to report GOH constitutive parameters estimated *in vivo* and *ex situ* simultaneously on the same subjects. In the following sections, the obtained results and study limitations are discussed.

Table 5: Results of the *in vivo* and *ex situ* parameter estimation for GOH model. In the *in vivo* case, for each animal, two sets of parameters are given. In the first set, all seven parameters were fitted. To obtain the second set, λ_z was fixed to the measured value and the other six parameters were fitted. In the *ex situ* case, parameters were estimated in three ways. Physiological (physiso.) rage is estimated based on the systolic pressure and 1:0.5 ratio is considered to be a physiological ratio. The coefficient of determination R^2 indicates the goodness of fit.

		μ [kPa]	k_1 [kPa]	k_2 [-]	α [deg]	κ [-]	H [mm]	λ_z [-]	R^2
S1R									
in vivo	λ_z fitted	214.9	483.6	0.0008	90	0.241	0.49	1.27	0.99
	λ_z fixed	223.9	364.1	0	61.3	0.179	0.48	1.29	0.99
ex situ	full range	18.6	57.1	5.54	0	0.300	-	-	0.88
	physio. range	11.3	14.1	1.40	34.4	0.000	-	-	0.95
	physio. range and ratio	25.2	5.2	6.52	0	0.113	-	-	0.99
S2L									
in vivo	λ_z fitted	255.3	44.8	0	65.1	0.000	0.60	2.00	0.96
	λ_z fixed	148.9	91.2	0	57.4	0.000	0.48	1.27	0.97
ex situ	full range	33.5	70.2	2.86	0	0.265	-	-	0.87
	physio. range	29.4	5.9	5.10	19.8	0.000	-	-	0.97
	physio. range and ratio	41.9	2.0	10.04	0	0.055	-	-	0.97
S2R									
in vivo	λ_z fitted	184.6	36.2	0	62.3	0.000	0.57	2.00	0.99
	λ_z fixed	89.6	75.1	0	52.7	0.000	0.47	1.22	0.99
ex situ	full range	58.8	3.9	10.26	0	0.123	-	-	0.95
	physio. range	28.9	4.0	6.98	16.7	0.002	-	-	0.95
	physio. range and ratio	42.8	4.4	7.16	11.4	0.040	-	-	0.96
S3L									
in vivo	λ_z fitted	218.2	37.5	0	65.7	0.000	0.63	2.00	0.99
	λ_z fixed	151.5	60.8	0	61.1	0.000	0.53	1.43	0.99
ex situ	full range	19.9	16.2	8.77	0	0.316	-	-	0.93
	physio. range	21.9	1.2	2.27	35.5	0.000	-	-	0.96
	physio. range and ratio	22.6	2.3	10.17	32.0	0.256	-	-	0.99

4.1. Data acquisition

Several limitations related to the data acquisition are important to note. Diastolic and systolic blood pressure were notably larger for sheep S1 than for

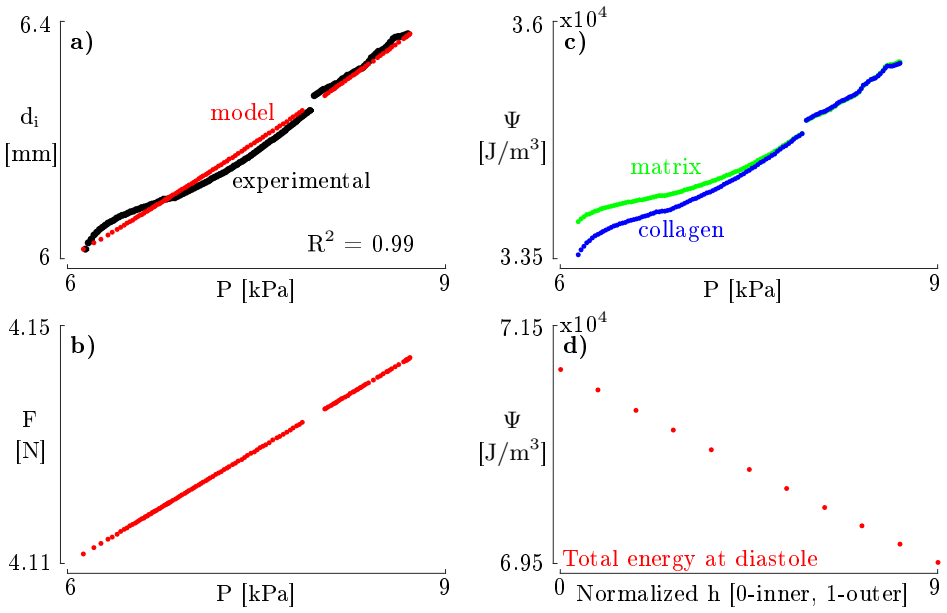

Figure 5: Results of the GOH *in vivo* fit for S3 left. The four minimized conditions are plotted in the following order: **a**) The *in vivo* measured pressure (P) and the inner diameter (d_i) data (black o) and the GOH model fit (red dots); **b**) Reduced axial force (F) predicted by the GOH model; **c**) Strain energy density (Ψ) - split into collagen and matrix contribution; **d**) Ψ throughout the aortic wall thickness (h) - from inner to outer wall.

sheep S2 and S3. The longer the animal is anesthetized, the bigger the pressure drop. We have previously investigated the effect of fitting different pressure ranges, from low to high, on the GOH material parameters. There was no substantial effect on any of the fitted parameters (unpublished data). However, this was done on idealized, simulated arteries with no smooth muscle tone and it is difficult to generalize this conclusion.

Furthermore, the biaxially tested samples were not fresh. They were slowly defrosted overnight prior to the testing day. The effect of freezing was studied in several different studies [31, 32, 33] on porcine and bovine arterial tissue. Contradictory results do not provide enough certainty to firmly conclude that the freezing has no effect on the mechanical behaviour of soft tissues. Hence, the parameters reported in our study should be interpreted with care.

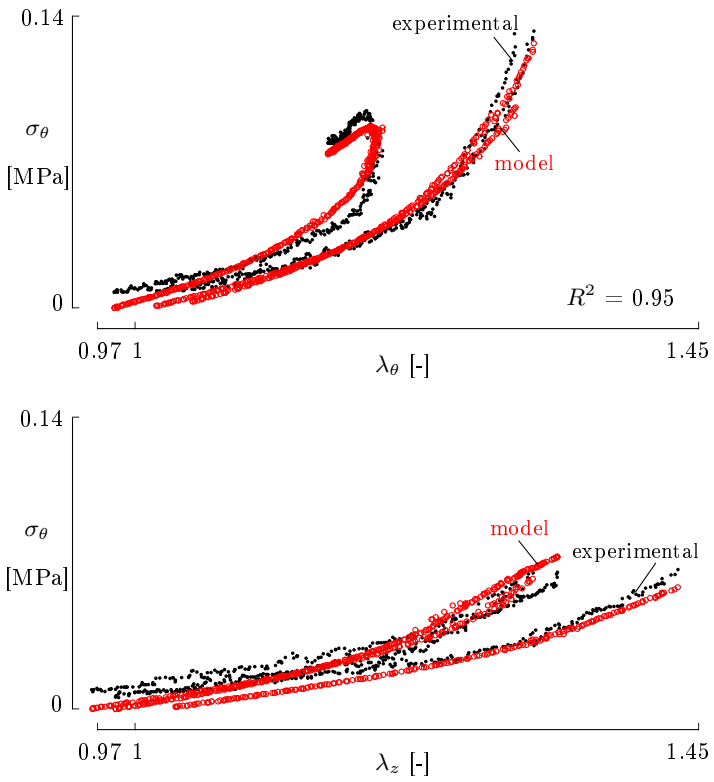

Figure 6: Experimental stress-stretch curves from zero to the physiological systolic stress level (dotted lines) and GOH model fit (circles) from S1R CCA. All three tested ratios are plotted.

4.2. In vivo material parameters

Both the MR and GOH material model were able to capture the behaviour of CCA, based on the *in vivo* measurements, which is reflected in high R^2 values. In most cases, the GOH model without k_2 had to be used. This was expected, since k_2 is a parameter which contributes more in the physiological pressure range and above. The measured pressure in our case was often below the diastolic value, due to the anesthetization of the animals.

For each material model, two fittings were performed: λ_z fitted and λ_z fixed to the experimentally measured value. In the former case of MR fitting, the obtained λ_z was overestimated when compared to the measured value. However, this overestimation was marginal. When the GOH model was used, λ_z often

went to the upper limit and it was preferred to have it fixed. These findings potentially show that a simpler model could be used for the estimation of the geometrical parameters such as λ_z, and the obtained results could be adopted for further characterization of the tissue with a more complex model.

4.3. Ex situ material parameters

In the case of *ex situ* parameter estimation, the MR material model was not able to capture the complex, nonlinear and anisotropic behaviour of the CCA in any of the three fitting approaches (full range, physiological range and physiological range and ratio). The resulting R^2 values ranged between 0.23 and 0.77. On the other hand, the GOH model performed well in all cases and resulted in R^2 values between 0.87 and 0.99.

When MR was used, in most of the cases, either parameter c_1 or c_2 ended up in the lower boundary, i.e. zero. This, once again, demonstrates that the model is not suitable for arterial tissue. In case of GOH, no evident trends were noticed for most of the parameters, when comparing different fitting approaches. To be able to entirely capture the anisotropic nature of the tissue, it is advised to use the full range of the data and multiple ratios for the parameter estimation.

4.4. In vivo vs. ex situ parameter estimation

The resulting parameters differ significantly between the two fitting approaches, i.e. *in vivo* vs. *ex situ*. In the absence of a ground truth, it is challenging to identify which method performs better, though advantages and drawbacks can be listed for both.

The obvious advantage of the *in vivo* method is the fact that the material is tested in its natural, physiological state, which is the state in which the parameters need to be known. However, a drawback of the parameter fitting method is the fact that the circumferential residual stress was not directly accounted for in the *in vivo* fitting approach. The current parameter approach assumes a stress-free reference state when the artery is at zero pressure and without axial prestretch. Including the circumferential residual stress, be it through the

addition of an opening angle or the incorporation of deposition stretches, as proposed by Bellini et al. [34], would add at least one additional parameter into the optimization procedure. This can lead to over-parametrization, as discussed in [20], but should definitely be investigated further. More measurement data can overcome this, but would necessitate the computationally less favourable approach of inverse finite elements, analogous to the approach proposed by Wittek et al. [21].

On the other hand, the *ex situ* fitting approach suffers from the fact that the tissue is no longer in its physiological state, despite typical measures taken to keep the tissue humid and at body temperature. Since no reagents were added to induce the vasodilation or vasoconstriction of the smooth muscle cells present in the media, their contribution will differ significantly compared to the physiological situation. Moreover, also here a reference state is considered that does not fully correspond to a zero stress state, since the tissue is flattened for the planar biaxial test. Again, ideally, an extra parameter accounting for this flattening should be included in the fitting procedure. Alternatively, extension-inflation tests could be performed, which resemble the *in vivo* loading conditions more closely. In the latter case, the challenge is to apply the correct axial prestretch and, as in the *in vivo* approach, to account for the circumferential residual strains.

Both methods suffered from the fact that a homogenization between the layers was considered, despite the distinct difference in mechanical behaviour of media and adventitia [35]. In the *in vivo* method, parameter fitting was performed based on the IMT ultrasound measurements. Since the adventitia is known to contribute mostly in the supra-physiological loading area, and the tissue was only probed at far lower pressures, one can deduce that mainly the medial properties were obtained in the *in vivo* case.

On the other hand, the *ex situ* approach considered the full thickness of the artery (IMAT), and also probed the tissue in supraphysiological loading, thereby activating the contribution of the adventitial layer. Therefore, this method would certainly benefit from a multilayered fitting approach, which will

again increase the number of fitting parameters. Badel and co-workers [36], for example, have suggested a multi-layered fitting approach for biaxial extension-inflation tests of arteries.

To the authors' knowledge, the only study that reported GOH material properties of sheep CCAs is the study by Dodson et al. [37]. They performed inflation-extension tests on fetal sheep CCAs as well as the imaging of the samples with second harmonic generation to visualize collagen and elastin content. Multiple pressure-diameter curves were fitted simultaneously with following parameters as the result: 3.85 kPa for μ, 26.7 kPa for k_1, 3.52 for k_2, 49.9 deg for α and 0.289 for κ. The reported α and κ from the imaging were 42.2 ± 11.2 and 0.286, respectively. Their parameters are closer to our *ex situ* parameters than to the *in vivo* ones which is to be expected. The reported μ is lower than our lowest result, while k_1 and k_2 are in the range with ours. The difference in μ can be attributed to the fact that in their case the fetal samples were tested which are expected to have lower stiffness of the arterial wall. Our *in vivo* α values were higher and *ex situ* ones mainly lower than the values reported by Dodson et al. [37].

4.5. Recommendations

Even if theoretically speaking both methods could be made to match, based on the recommendations in the previous section, both methods also suffer from noise and measurement acquisition errors, which should be minimized or accounted for as suggested below.

For the *in vivo* approach, the *in vivo* pressure-diameter measurements should be done as soon as possible after the animal is anesthetized to keep the pressure as high as possible. Drugs for blood pressure increase could be administered, although these can result in less regular pressure and diameter patterns which can be more challenging to synchronize if not recorded simultaneously. Simultaneous acquisition is preferred but often not applicable in clinical scenarios. Data from at least three but preferably more cardiac cycles should be obtained and averaged, to compensate for breathing effects and other measurement noise.

In this study, this was the case for the pressure measurements but not for the diameter measurements.

In the *ex situ* approach, care should be taken to test the tissue in conditions that mimic the physiological situation as closely as possible. Also, care should be taken to induce a homogeneous loading situation, or when this is not possible, to correct for the inhomogeneities or take them into account through full field strain mapping [38, 39, 26].

5. Conclusion

An experimental material parameter estimation requires excision of the samples which is an invasive procedure and can not be applied preoperatively. However, the *in vivo* patient-specific estimation of the same parameters comes with its own challenges, stemming from the fact that limited information is available *in vivo*. In this study the *in vivo* material parameters estimated with the approach proposed by Smoljkic et al. [20] were compared to parameters obtained experimentally from planar biaxial tests.

In the absence of a ground truth, and with clear advantages and disadvantages to both approaches, the difference in the results can be attributed to a number of factors, including the obvious difference in applied loading regime. An important direction for future work is the correct definition of the tissue's reference state, both in the *in vivo* and *ex situ* case, thereby incorporating residual stresses, as well as accounting for the layer-specificity of arterial tissue.

Acknowledgements.

This work was supported by a research project (G093211N), a postdoctoral fellowship (PD0-12) of the Research Foundation-Flanders (FWO), and by a grant from the Croatian Science Foundation (project IP-2014-09-7382 I. Karšaj). The authors would like to thank Alvaro Jorge-Peñas for developing the marker tracking software.

Declaration statement.

The authors have no competing interests to declare.

References

[1] Kuroda, Y., Akiyama, H., Nankaku, M., So, K. **A Report on Three Consecutive Cases using Computer Tomography 3D Preoperative Planning for Conversion of Arthrodesed Hips to Total Hip Replacements**. *HSS Journal* 2015;11:76–83 DOI:10.1007/s11420-014-9423-7

[2] Imai, H., Miyawaki, J., Kamada, T., Takeba, J. **Preoperative planning and postoperative evaluation of total hip arthroplasty that takes combined anteversion**. *Eur J Orthop Surg Traumatol.* 2016;26:493–500 DOI:10.1007/s00590-016-1777-8

[3] Franceschi, J., Sbihi, A., Orthopedic, A., France, S. **Total knee arthroplasty: Postoperative CT-based assessment of implant positioning**. *Orthop Traumatol Surg Res.* 2014;100:S281–S286 DOI:10.1016/j.otsr.2014.04.003

[4] Ettinger, M., Claassen, L., Paes, P., Calliess, T. **2D versus 3D templating in total knee arthroplasty**. *Knee* 2016;23:149–151. DOI:10.1016/j.knee.2015.08.014

[5] Chen, J., Zhang, Z., Chen, X. **Design and manufacture of customized dental implants by using reverse engineering and selective laser melting technology**. *J Prosthet Dent.* 2014;112:1088–1095.e1 DOI:10.1016/j.prosdent.2014.04.026

[6] Schepers, R. H., Raghoebar, G. M., Vissink, A., Stenekes, M. W., Kraeima, J., Roodenburg, J. L., Reintsema, H., Witjes, M. J. **Accuracy of fibula reconstruction using patient-specific CAD/CAM reconstruction**

plates and dental implants: A new modality for functional reconstruction of mandibular defects. *J Craniomaxillofac Surg.* 2015;43:649–657 DOI:10.1016/j.jcms.2015.03.015

[7] Steinbacher, D. M. **Three-Dimensional Analysis and Surgical Planning in Craniomaxillofacial Surgery**. *J Oral Maxillofac Surg.* 2015;73:S40–S56 DOI:10.1016/j.joms.2015.04.038

[8] Vale, F., Scherzberg, J., Cavaleiro, J., Sanz, D., Caramelo, F., Maló, L., Marcelino, J. P. **3D virtual planning in orthognathic surgery and CAD/CAM surgical splints generation in one patient with craniofacial microsomia: a case report**. *Dental Press J Orthod.* 2016;21:89–100 DOI:10.1590/2177-6709.21.1.089-100.oar

[9] von Sachsen, S., Senf, B., Burgert, O., Meixensberger, J., Florek, H. J., Mohr, F. W., Etz, C. D. **Stent graft visualization and planning tool for endovascular surgery using finite element analysis**. *Int J Comput Assist Radiol Surg.* 2014;9:617–633 DOI:10.1007/s11548-013-0943-2

[10] Perrin, D., Badel, P., Orgéas, L., Geindreau, C., Dumenil, A., Albertini, J.-N., Avril, S. **Patient-specific numerical simulation of stent-graft deployment: Validation on three clinical cases**. *J Biomech.* 2015;48:1868–1875 DOI:10.1016/j.jbiomech.2015.04.031

[11] Iannaccone, F., De Beule, M., De Bock, S., Van der Bom, I. M. J., Gounis, M. J., Wakhloo, A. K., Boone, M., Verhegghe, B., Segers, P. **A Finite Element Method to Predict Adverse Events in Intracranial Stenting Using Microstents: In Vitro Verification and Patient Specific Case Study**. *Ann Biomed Eng.* 2016;44:442–452 DOI:10.1007/s10439-015-1505-2

[12] Bateman, M. G., Hill, A. J., Quill, J. L., Iaizzo, P. A. **The Clinical Anatomy and Pathology of the Human Arterial Valves: Implications for Repair or Replacement**. *J Cardiovasc Transl Res.* 2013;6:166–175 DOI:10.1007/s12265-012-9438-8

[13] Sun, Z.-H. **Abdominal aortic aneurysm: Treatment options , image visualizations and follow-up procedures**. *J Geriatr Cardiol.* 2012;9:49–60 DOI:10.3724/SP.J.1263.2012.00049

[14] Pierce, D. M., Maier, F., Weisbecker, H., Viertler, C., Verbrugghe, P., Famaey, N., Fourneau, I., Herijgers, P., Holzapfel, G. A. **Human thoracic and abdominal aortic aneurysmal tissues: Damage experiments, statistical analysis and constitutive modeling**. *J Mech Behav Biomed Mater.* 2015;41:92–107 DOI:10.1016/j.jmbbm.2014.10.003

[15] Sacks, M. S. **Biaxial mechanical evaluation of planar biological materials**. *J Elasticity* 2000;61:199–246 DOI:10.1023/A:1010917028671

[16] Famaey, N., Sommer, G., Vander Sloten, J., Holzapfel, G. A. **Arterial clamping: finite element simulation and in vivo validation**. *J Mech Behav Biomed Mater.* 2012;12:107–118 DOI:10.1016/j.jmbbm.2012.03.010

[17] Schulze-Bauer, C. A. J., Holzapfel, G. A. **Determination of constitutive equations for human arteries from clinical data**. *J Biomech.* 2003;36:165–169 DOI:10.1016/S0021-9290(02)00367-6

[18] Stålhand, J., Klarbring, A., **Aorta in vivo parameter identification using an axial force constraint**. *Biomech Model Mechanobiol.* 2005;3:191–199 DOI:10.1007/s10237-004-0057-4

[19] Masson, I., Boutouyrie, P., Laurent, S., Humphrey, J. D., Zidi, M. **Characterization of arterial wall mechanical behavior and stresses from human clinical data**. *J Biomech.* 2008;41:2618–2627 DOI:10.1016/j.jbiomech.2008.06.022

[20] Smoljkić, M., Vander Sloten, J., Segers, P., Famaey, N. **Non-invasive, energy-based assessment of patient-specific material properties of arterial tissue**. *Biomech Model Mechanobiol.* 2015;14:1045–1056 DOI:10.1007/s10237-015-0653-5

[21] Wittek, A., Karatolios, K., Bihari, P., Schmitz-Rixen, T., Moosdorf, R., Vogt, S., Blase, C. **In vivo determination of elastic properties of the human aorta based on 4D ultrasound data**. *J Mech Behav Biomed Mater.* 2013;27:167–183 DOI:10.1016/j.jmbbm.2013.03.014

[22] Larsson, M., Kremer, F., Claus, P., Kuznetsova, T., Brodin, L.-A., D'hooge, J. **Ultrasound-based radial and longitudinal strain estimation of the carotid artery: a feasibility study**. *IEEE Trans Ultrason Ferroelectr Freq Control.* 2011;58:2244–2251 DOI:10.1109/TUFFC.2011.2074

[23] Widman, E. , Caidahl, K., Heyde, B., D'hooge, J., Larsson, M. **Ultrasound speckle tracking strain estimation of in vivo carotid artery plaque with in vitro sonomicrometry validation**. *Ultrasound Med Biol.* 2015;41:77–88 DOI:10.1016/j.ultrasmedbio.2014.06.013

[24] Koelwyn, G. J., Currie, K. D., MacDonald, M. J., Eves, N. D. **Ultrasonography and tonometry for the assessment of human arterial stiffness, applied aspects of ultrasonography in humans**. In: Ainslie, P., editor. Applied Aspects of Ultrasonography in Humans, *InTech*, 2012, p. 115–140 DOI:10.5772/39193

[25] Nielsen, P. M. F., Hunter, P. J., Smaill, B. H. **Biaxial Testing of Membrane Biomaterials: Testing Equipment and Procedures**. *J Biomech Eng* 1991;113:295–300 DOI:10.1115/1.2894887

[26] Fehervary, H., Smoljkić, M., Vander Sloten, J., Famaey, N. **Planar biaxial testing of soft biological tissue using rakes: a critical analysis of protocol and fitting process**. *J Mech Behav Biomed Mater.* 2016;61:135–151 DOI:10.1016/j.jmbbm.2016.01.011

[27] Gasser, T. C., Ogden, R. W., Holzapfel, G. A. **Hyperelastic modelling of arterial layers with distributed collagen fibre orientations**. *J R Soc Interface.* 2006;3:15–35 DOI:10.1098/rsif.2005.0073

[28] Weisbecker, H., Pierce, D. M., Regitnig, P., Holzapfel, G. A. **Layer-specific damage experiments and modeling of human thoracic and abdominal aortas with non-atherosclerotic intimal thickening**, *J Mech Behav Biomed Mater.* 2012;12:93–106 DOI:10.1016/j.jmbbm.2012.03.012

[29] Ogden, R.W. **Anisotropy and Nonlinear Elasticity in Arterial Wall Mechanics**. In: Holzapfel, G.A., Ogden R.W., editors. Biomechanical Modelling at the Molecular, Cellular and Tissue Levels, *Springer Vienna*, 2009, p. 179–258 DOI:10.1007/978-3-211-95875-9_3

[30] Smoljkić, M., Fehervary, H., Van den Bergh, P., Jorge-Peñas, A., Kluyskens, L., Dymarkowski, S., Verbrugghe, P., Meuris, B., Vander Sloten, J., Famaey, N. **Biomechanical Characterization of Ascending Aortic Aneurysms**, *Biomech Model Mechanobiol.*, 2017;16:705-720 DOI:10.1007/s10237-016-0848-4

[31] Venkatasubramanian, R. T., Grassel, E. D., Barocas, V. H., Lafontaine, D., Bischof, J. C. **Effects of Freezing and Cryopreservation on the Mechanical Properties of Arteries**. *Ann Biomed Eng.* 2006;34:823–832 DOI:10.1007/s10439-005-9044-x

[32] Stemper, B. D., Yoganandan, N., Stineman, M. R., Gennarelli, T. A., Baisden, J. L., Pintar, F. A. **Mechanics of Fresh, Refrigerated, and Frozen Arterial Tissue**. *J Surg Res.* 2007;139:236–242 DOI:10.1016/j.jss.2006.09.001

[33] Chow, M.-J., Zhang, Y. **Changes in the Mechanical and Biochemical Properties of Aortic Tissue due to Cold Storage**, *J Surg Res.* 2011;171:434–442 DOI:10.1016/j.jss.2010.04.007

[34] Bellini, C., Ferruzzi, J., Roccabianca, S., DiMartino, E.S., Humphrey, J.D. **A Microstructurally Motivated Model of Arterial Wall Mechanics with Mechanobiological Implications**, *Ann Biomed Eng.* 2014;42:488–502 DOI:10.1007/s10439-013-0928-x.A

[35] Holzapfel, G. A., Sommer, G., Gasser, C. T., Regitnig, P. **Determination of layer-specific mechanical properties of human coronary arteries with nonatherosclerotic intimal thickening and related constitutive modeling**, *Am J Physiol Heart Circ Physiol.* 2005;289:2048–2058 DOI:10.1152/ajpheart.00934.2004.

[36] Badel, P., Avril, S., Lessner, S., Sutton, M. **Mechanical identification of layer-specific properties of mouse carotid arteries using 3D-DIC and a hyperelastic anisotropic constitutive model**. *Comput Methods Biomech Biomed Engin.* 2012;15:37–48 DOI:10.1080/10255842.2011.586945

[37] Dodson, R. B., Rozance, P. J., Reina-Romo, E., Ferguson, V. L., Hunter, K. S. **Hyperelastic remodeling in the intrauterine growth restricted (iugr) carotid artery in the near-term fetus**. *J Biomech.* 2013;46:956–963 DOI:http://dx.doi.org/10.1016/j.jbiomech.2012.12.013

[38] Kim, J.-H., Avril, S., Duprey, A., Favre, J.-P., **Experimental characterization of rupture in human aortic aneurysms using a full-field measurement technique**. *Biomech Model Mechanobiol.* 2012;11:841–853 DOI:10.1007/s10237-011-0356-5

[39] Palanca, M., Tozzi, G., Cristofolini, L. **The use of digital image correlation in the biomechanical area : a review**. *International Biomechanics* 2015;3:1–21 DOI:10.1080/23335432.2015.1117395